International Journal of Heat and Mass Transfer 52 (2009) 1761–1768

Contents lists available at ScienceDirect

International Journal of Heat and Mass Transfer

journal homepage: www.elsevier.com/locate/ijhmt

Vascular structures with flow uniformity and small resistance

J. Lee [a], S. Lorente [b], A. Bejan [c,*], M. Kim [a]

[a] Pohang University of Science and Technology, Department of Mechanical Engineering, San 31, Hyoja-dong, Nam-gu, Pohang, Kyoungbuk 790-784, South Korea
[b] Université de Toulouse, UPS, INSA, LMDC (Laboratoire Matériaux et Durabilité des Constructions), 135, Avenue de Rangueil, F-31 077 Toulouse Cedex 04, France
[c] Duke University, Department of Mechanical Engineering and Materials Science, Durham, NC 27708-0300, USA

ARTICLE INFO

Article history:
Received 12 August 2008
Received in revised form 18 September 2008
Available online 26 December 2008

Keywords:
Vascularized materials
Tree designs
Dendritic
Constructal
Multi-functional
Multi-scale
Self-healing
Self-cooling

ABSTRACT

The drive toward vascular smart materials calls for novel flow architectures that bathe and serve entire volumes and areas as uniformly as possible. Here, we show that vascular designs consisting of trees matched canopy to canopy can be configured so that they have two qualities: small flow resistance (ψ) and small volumetric flow nonuniformity (μ). In the past, the only quality sought was small flow resistance. Two classes of architectures are explored: (a) matched trees with diagonal channels through the core and (b) matched trees with orthogonal channels. First, we show that flow architectures can be developed and selected for minimum flow nonuniformity alone. Second, in the $\psi - \mu$ design space the best of designs (b) lie close to the best of designs (a), although the best of designs (b) offer slightly better configurations (low ψ and μ) than the best of designs (a). Comparisons with similar architectures generated based on genetic algorithms show that the minimum global flow resistance ψ of designs (a,b) is 2–5 times smaller than the genetic-algorithm values. The flow nonuniformities μ corresponding to the minimum ψ of designs (a,b) are 2–70 times smaller than the flow nonuniformities of the genetic-algorithm results.

1. Introduction

The newest work on the frontiers of thermal sciences and technology calls for innovative designs of distributed energy systems and models and methods that resemble those used in the analysis of biological (living) bodies [1]. An important movement on the frontier is the evolution of technology toward compact flow structure with greater *volumetric* densities of heat transfer, mass transfer and chemical reaction rates. This is generating new kinds of flow architectures where the basic flow configuration consists of trees and superpositions of trees (i.e. grids). The reason is that the tree-shaped flow is the configuration that offers greatest access between the volume that must be bathed and the port through which the stream enters or exits the volume [2]. Vascular designs with trees matched canopy to canopy were proposed for thermofluids engineering at the start of constructal theory [2,3], and have now spread through many sectors such as the cooling of electronics, the packaging of fuel cells, and the development of embedded vasculatures for smart materials with volumetric functionalities such as self-healing and self-cooling [3–17]. The growth of the field was reviewed most recently in Refs. [18,19].

A body with embedded tree-shaped flows that bathe the entire volume is a vascularized body. Materials with such constitution have properties unlike those of classical designs, where the flow structure has a single scale that is distributed uniformly through the volume (e.g., parallel channels, parallel tubes in crossflow, homogeneous porous media). Vascularized materials are generating their own thermofluids science: the driving force is the need to know the new properties of the architecture and the various measures of flow and transport performance. The most basic outcome of this new work is the emergence of a thermodynamics in which nonequilibrium (i.e. flow) systems are no longer black boxes. They are thermodynamic systems with configuration [20].

The way to bathe a volume with a single stream is to invade it as river-delta tree, and later to drain it as a river-basin tree. The resulting architecture then must resemble two trees matched canopy to canopy. Two examples are given in Fig. 1. Matched trees have been proposed and optimized for volumetric cooling [2,3] and for the repairing of cracks distributed randomly through the volume [21]. They have also been applied to the design of compact heat sinks and heat exchangers [11–14].

Lee et al. [22] showed that grids with diagonal channels through the middle and orthogonal channels on the perimeter (Fig. 1a) can be designed to have lower global resistances than grids with orthogonal channels everywhere (Fig. 1b). Here, we show that in both designs the flow rates through the grid channels are distributed nonuniformly. The maldistribution is significant. For example, if $\dot{m}_{max}$ and $\dot{m}_{min}$ are the largest and smallest mass flow rates through the inner channels including the corner channels in the

* Corresponding author. Tel.: +1 919 606 5309; fax: +1 919 660 8963.
E-mail address: abejan@duke.edu (A. Bejan).

0017-9310/$ - see front matter © 2008 Elsevier Ltd. All rights reserved.
doi:10.1016/j.ijheatmasstransfer.2008.09.027

Nomenclature

A	area, m^2
C	factor, Eq. (1)
d	elemental length scale, m
D_i	channel diameter, m
L	length of square domain, m, Figs. 1, 5 and 8
L_i	channel length, m
$\dot{m}$	mass flow rate, kg s^{-1}
N	number of *d-elements* in one direction
Sv	svelteness number, Eq. (2)
Re	Reynolds number
V	total volume, m^3
V_f	total flow volume, m^3
x, y, z	coordinates

Greek symbols

ΔP	pressure difference, Pa
ν	kinematic viscosity, m^2 s^{-1}
ϕ	porosity
μ	dynamic viscosity, N s m^{-2}
μ	flow rate nonuniformity
ψ	nondimensional global flow resistance, Eqs. (4) and (7)
∞	infinity

Subscripts

i	channel rank
f	fluid
max	maximum
min	minimum
2D	two-dimensional definition

grid, and if the designs have a single channel diameter, then the designs of Fig. 1a and b exhibit significant flow nonuniformity: $\dot{m}_{max}/\dot{m}_{min} = 35.95$ and 4.04, respectively. Flow rate nonuniformity is a negative feature in the design of vascularized self-healing materials, because the chief function of the grid is to give every volume element of the material access to the healing fluid supply. It is also a negative feature in the design of volumetric cooling for surfaces and bodies, where flowing coolant is needed at every point.

The fundamental design question that emerges out of this difficulty is how to configure vascular grids so that they have two important qualities at the same time: small global flow resistance and minimal flow nonuniformity. The vasculature that emerges is a two-objective architecture and joins ranks with other multi-objective natural designs (e.g., lungs, muscles [23,24]) and dendritic heat exchangers [12,25,26].

2. Model

The model was selected in order to make the results comparable with the flow regime required for self-healing flow designs (Reynolds numbers of order 1), and the designs that have been optimized and reported until now [21,22,27]. The flow in every channel (i) is in the Poiseuille regime,

$$\Delta P_i = C\dot{m}_i \frac{L_i}{D_i^4} \tag{1}$$

where ΔP_i, $\dot{m}_i$, L_i, and D_i represent the pressure drop along the channel, the mass flow rate, the channel length, and the channel hydraulic diameter. The factor C depends on the shape of the channel cross-section, for example $C = 128\nu/\pi$ for a round cross-section, in which case D_i is the cross-section diameter.

Pressure losses at junctions, bifurcations and bends are neglected based on the assumption that the svelteness (Sv) of the flow architecture is sufficiently large (Sv >> 10, in an order of magnitude sense). The svelteness is a global property of the flow architecture, which is defined as [28]

$$\mathrm{Sv} = \frac{\text{external length scale}}{\text{internal length scale}} = \frac{L}{V_f^{1/3}} \tag{2}$$

The external length scale L is the side of the square slab shown vascularized in Fig. 1. The smallest length scale of the design is the side (d) of the square elements touched by the channels of the grid. A basic design requirement is that every d-element must have access to fluid that flows. The global scale $L \times L$ is represented alternatively by $N \times N$, where N is the number of d-elements counted in one of the cartesian directions ($L = Nd$).

The volume occupied by the flow (V_f) is fixed. If the thickness of the slab is d, then $V = L^2 d$, and this means that fixing the flow volume V_f is equivalent to fixing the porosity

$$\phi = \frac{V_f}{V} \tag{3}$$

In this nomenclature, the svelteness becomes $\mathrm{Sv} = (L/\phi \mathrm{d})^{1/3}$. Flow structures with slender channels ($L/d >> 1$) and small porosity are svelte. Note that the svelteness of the flow architecture is not the same as the slenderness of one channel or the porosity of the vascular body.

For every grid architecture such as Fig. 1a, we calculated two global measures of performance. First, the overall flow resistance of the grid is expressed in dimensionless form as [21]

$$\psi = \frac{\Delta P}{C\dot{m}}\phi^2 d^3 \tag{4}$$

where ΔP is the overall pressure drop, and $\dot{m}$ is the total mass flow rate that proceeds from one corner of the slab to the other. The second global measure of performance is the flow nonuniformity ratio

$$\mu = \frac{\dot{m}_{max}}{\dot{m}_{min}} \tag{5}$$

where $\dot{m}_{max}$ and $\dot{m}_{min}$ represent the largest and smallest mass flow rates present in channels that sweep across the slab and touch the inner volume elements (e.g., channels 10,...,28 in Fig. 1a, and channels 11–20 in Fig. 1b). The peripheral channels have necessarily larger flow rates because they act as supply routes, and are not considered in the calculation of μ.

A uniform distribution ($\mu = 1$) can be achieved in the inner channels by properly tapering the peripheral supply channels [2]. Such a technique is not workable at the small scales that are envisaged for self-healing vasculatures ($D < 100$ μm), where channels have constant thickness because they are made by ink writing techniques [29]. The challenge is to reduce μ by working with channels of constant thickness, for example, by placing thin channels (D_1) across the inner field, and thicker channels (D_2) along the periphery.

The μ ratio is a "global" property because it characterizes the entire flow architecture, no matter where $\dot{m}_{max}$ and $\dot{m}_{min}$ occur. Other global properties of the flow architecture are ψ, Sv and ϕ.

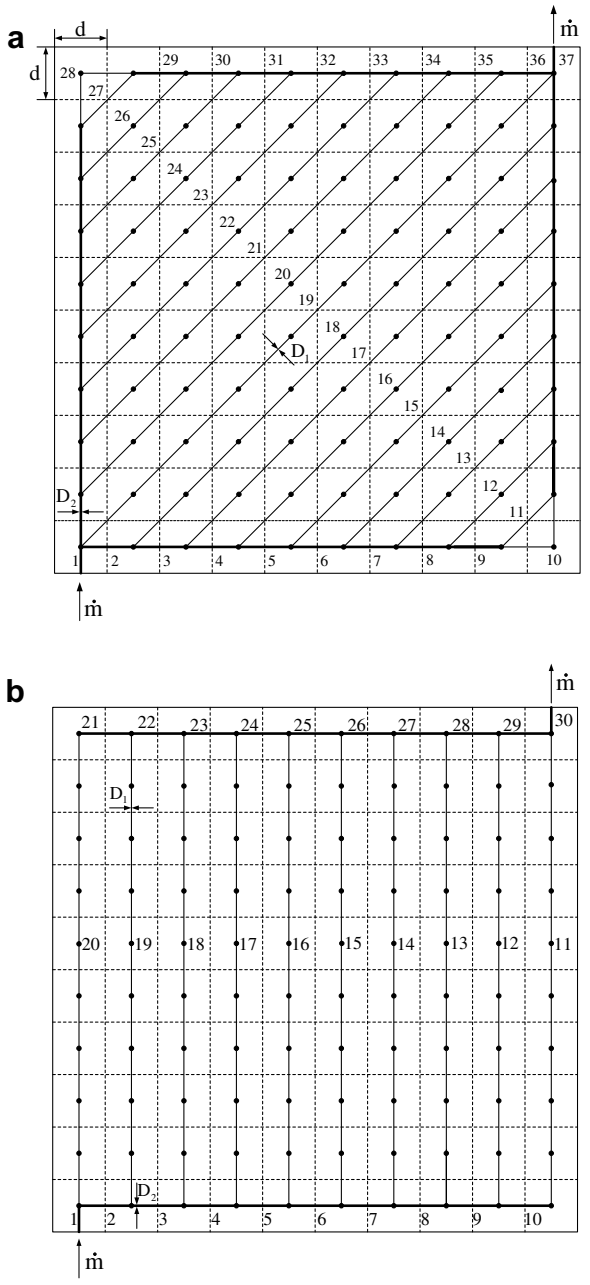

Fig. 1. Trees matched canopy to canopy: (a) diagonal channels through the core and (b) orthogonal channels.

3. Flow distribution in grids with minimum flow resistance

The nonuniformity of the flow distribution becomes evident if we focus on the flow resistance alone, and minimize ψ. The only degree of freedom in the designs of Fig. 1a and b is the channel diameter ratio D_1/D_2. The calculation of $\Delta P/\dot{m}$ (or ψ) consists of invoking Eq. (1) for all the channels, accounting for mass continuity at every junction, and adding all the ΔP_i's along one flow path from the inlet to the outlet of the flow structure. The technique is detailed in Ref. [22] and is not repeated here. The ψ function determined in this manner has a single value for an assumed configuration. The ψ value calculated for Fig. 1a reaches the minimum value 2.13 when $D_1/D_2 = 0.481$.

This calculation was performed for many configurations by changing the ratio D_1/D_2. The flow rates ($\dot{m}$) through all the channels of the minimum-ψ configuration are shown in Fig. 2a. The

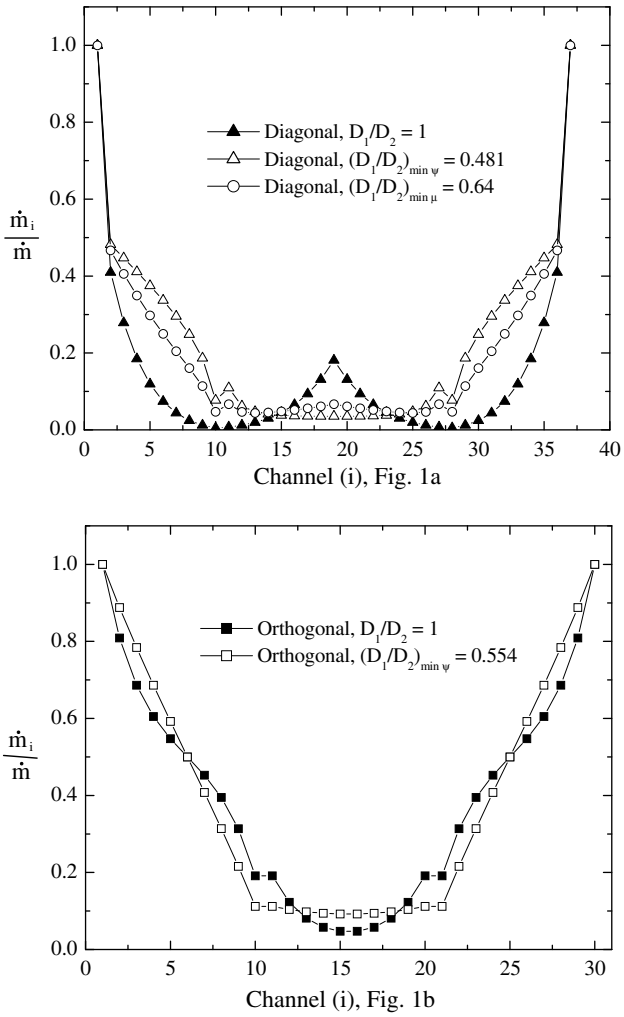

Fig. 2. The distribution of flow rates in the designs of Fig. 1.

flow rates are the smallest through the inner channels (numbered 11–28), and show a certain degree of nonuniformity: the nonuniformity ratio for the inner channels is $\mu = \dot{m}_{11}/\dot{m}_{18} = 3.09$. Because of symmetry, $\dot{m}_{11}$ and $\dot{m}_{18}$ are the same mass flow rates as $\dot{m}_{27}$ and $\dot{m}_{20}$, respectively.

Fig. 2a also shows the distribution of flow rates when the design of Fig. 1a has channels with one diameter, $D_1 = D_2$. The global flow resistance in this case is larger, $\psi = 4.67$, and so is the maldistribution, $\mu = \dot{m}_{19}/\dot{m}_{10} = 35.95$.

Fig. 2b shows the corresponding results for the configuration with orthogonal channels (Fig. 1b). When the flow resistance is minimum ($\psi = 2.17$), the optimal ratio of channel sizes is $D_1/D_2 = 0.554$, and the flow nonuniformity is $\mu = \dot{m}_{11}/\dot{m}_{15} = 1.22$. When the channels have the same diameter ($D_1 = D_2$) the values of ψ and $\mu (= \dot{m}_{10}/\dot{m}_{15})$ are 5.29 and 4.04, respectively.

4. Less flow nonuniformity and less global resistance

The results of Fig. 2a and b suggest that reductions in ψ go hand in hand with reductions in μ. We investigated this further, and found that this is not true in general. Fig. 3 shows that ψ and μ do not always change in the same direction when we change the flow configuration.

In summary, Fig. 2a and b show that the diagonal pattern is better than the orthogonal pattern for achieving greater flow access (lower ψ). The orthogonal pattern is better for archiving flow uniformity (lower μ).

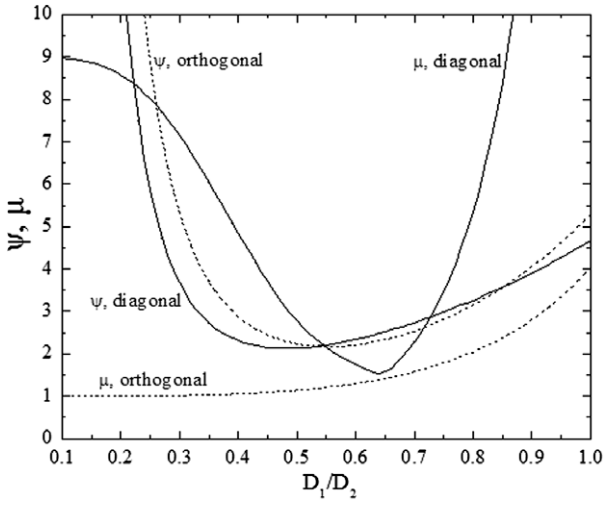

Fig. 3. The global flow resistance and flow nonuniformity of the designs of Fig. 1a and b as functions of the channel size ratio.

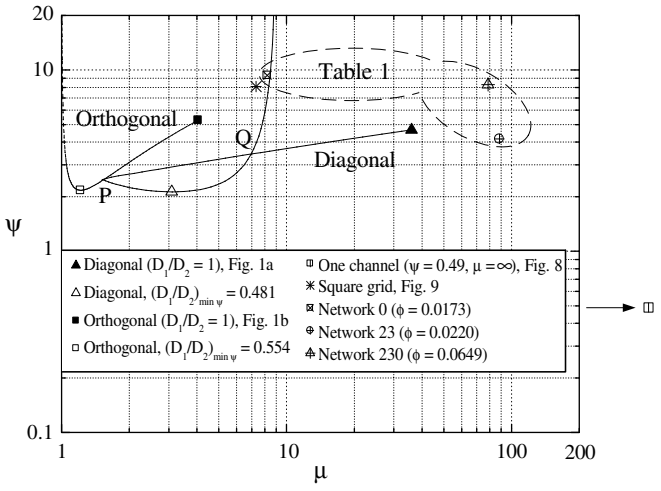

Fig. 4. The global flow resistance and nonuniformity of the designs of Fig. 1a and b, and Table 1.

The three (ψ,μ) designs reported in Fig. 2a and b are represented by three points on the two solid curves in Fig. 4. The two points plotted for grids with diagonal channels are for the designs that have $D_1/D_2 = 1$ and optimal D_1/D_2 for minimum ψ. These two points fall on one curve, which is the locus of the configurations of Fig. 1a covering the entire range of D_1/D_2 values. On this curve, note point P where the flow rate nonuniformity is minimum. Fig. 3 showed that this design has the diameter ratio $D_1/D_2 = 0.64$ and $\psi = 2.48$ and $\mu(=\dot{m}_{11}/\dot{m}_{13}) = 1.51$. The distribution of flow rates in the configuration with $D_1/D_2 = 0.64$ was shown in Fig. 2a. The solid curve crosses itself at point Q ($\psi = 3.43, \mu = 6.97$), which corresponds to two diagonal designs with $D_1/D_2 = 0.31$ and 0.83.

Designs with orthogonal channels offer a somewhat different two-objective performance. The two designs of Fig. 2b are represented by the two (ψ,μ) points marked on the orthogonal curve in Fig. 4. These points are linked by the curve along which D_1/D_2 varies. Fig. 3 shows the way in which ψ and μ vary as D_1/D_2 changes.

5. Discussion

The conclusion drawn based on Fig. 4 is that the best orthogonal designs promise slightly better two-objective performance than the best diagonal designs. The closest orthogonal-design points lie closer to the origin of the $\psi - \mu$ frame than the closest point of the diagonal designs. The challenge is to discover even better configurations. Can the flow architecture morph such that the points of Fig. 4 migrate even close to the origin of the $\psi - \mu$ frame?

An alternate approach to the discovery of vasculatures for bathing a square slab was developed in Ref. [27]. As in Fig. 1, the size and graininess of the tree–tree flow structure (10×10) were fixed, however the channel volume was distributed based on a genetic algorithm with a different set of objectives: minimum corner to corner flow resistance, and minimum total channel volume. Three orthogonal designs are summarized in Table 1. They come from a much larger body of results [27], which shows qualitatively that on a field of global flow resistance (y) versus total channel volume (x) the designs evolve from above toward a bottom curve $y(x)$ with negative slope and positive curvature (Fig. 6) [30]. The designs occupy the half-domain situated above the $y(x)$ curve. They migrate in time toward the solid curve, which represents the locus of "equilibrium flow configurations" [20]. These are the configurations that are the most free to morph: for them the global performance has become stationary even though there are many configurations that perform at or near this level. The time arrow of evolution of configuration is the direction (the tendency) of the phenomenon of generation of flow configuration.

The three designs shown in Table 1 were evaluated in dimensional terms in Ref. [27] by using $L = 1$ cm, round cross-sections with $D_1 = 100$ μm and $D_2 = 200$ μm, $\mu = 1.005 \times 10^{-3}$ Ns/m^2 (water liquid at 20 °C), and a total flow rate of 20 ml/min, which corresponds to $\dot{m} = 0.333$ g/s. These designs are directly comparable with the orthogonal design with $D_1/D_2 = 0.5$ in Fig. 4, which is a point situated very close to the minimum of the "orthogonal" curve (see the white square). A special case is network 0 shown in Fig. 5, which has channels with a single diameter ($D = 100$ μm). The channel volume fraction that was minimized in Ref. [27] was defined based on a two-dimensional projection,

$$\phi_{2D} = \frac{A_f}{A} = \frac{1}{L^2}\sum_i D_i L_i \tag{6}$$

where L is the length of the square domain and A_f is the area occupied by all the channels when projected on the face of the slab ($A = L \times L$). Note that the area function ϕ_{2D} is not the same as the porosity ϕ defined in Eq. (3). In Table 1 we listed both ϕ and ϕ_{2D}.

As we indicated in Fig. 6, the three cases of Table 1 show that the minimized ΔP decreases when the minimized ϕ_{2D} increases. This means that the three designs lie close to the border occupied by the equilibrium flow structures. This monotonic relationship between ΔP and ϕ_{2D} might be expected from Eq. (4), except that in the present case the channel volume is represented by ϕ_{2D}, not ϕ. The assumption of Poiseuille flow in every channel, which

Table 1
The geometrical parameters and total pressure drop of the networks shown in Fig. 5 ($V = 100$ mm^3, $A = 100$ mm^2) [27].

Network	V_f (mm^3)	A_f (mm^2)	ϕ	ϕ_{2D}	ΔP (Pa)	ψ	ψ_{2D}	μ
0	1.73	22	0.0173	0.220	427,569	9.34	73.32	8.21
23	2.20	24	0.0220	0.240	117,868	4.17	28.62	88.29
230	6.49	42.2	0.0649	0.422	26,947	8.30	62.55	78.58

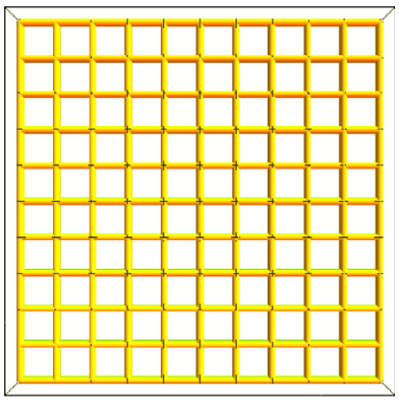

Network 0

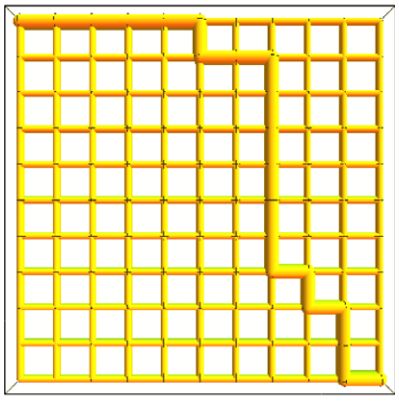

Network 23

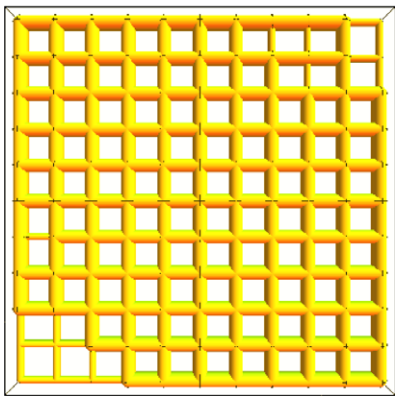

Network 230

Fig. 5. The three designs presented in Table 1.

is the basis for the dimensionless flow-resistance group ψ in Eq. (4), also applies when the channel volume fraction is represented by ϕ_{2D}. The resulting flow-resistance group based on ϕ_{2D} is

$$\psi_{2D} = \frac{\Delta P}{C\dot{m}}\phi_{2D}^4 d^3 \tag{7}$$

This group is also listed in Table 1, and shows that it is essentially a number of order 10^2 while the ΔP values vary much more widely.

The new aspect of flow performance considered in this paper is the nonuniformity of the distribution of flow rate over the central portion of the vascular body, and how to decrease the flow nonuniformity. We calculated μ for the three cases of Fig. 5 by identifying the highest and lowest flow rates that cross the diagonal plane stretching from the lower-left corner to the upper-right corner. The μ values are based on Eq. (5), and listed in Table 1.

The flow nonuniformity μ adds a third dimension (z) to the design space sketched in Fig. 6. The work summarized in Fig. 4 fits in the constant-x plane because it was based on as the assumption that the total channel volume is fixed. We have expanded Fig. 4 by adding the three designs that correspond to Table 1 in $\psi - \mu$ coordinates. When compared with the diagonal and orthogonal designs, the three designs are inferior in both respects flow resistance and flow nonuniformity. The flow resistances ψ of Table 1 exceed by factors greater than 3 the flow resistances of the best of the designs based on Fig. 1a and b. The flow nonuniformities μ of Table 1 exceed by factors of order 100 the flow nonuniformities of the best diagonal and orthogonal designs.

These conclusions do not change if the comparison of Fig. 4 is expressed in terms of the ψ_{2D} definition, Eq. (7). This alternative is presented in Fig. 7, where the discrepancy between the flow resistances (ψ_{2D}) of Table 1 and the best designs of Fig. 1a and b is a factor of order 10. The flow nonuniformities are described by the same μ values as in Fig. 4.

Why are the discrepancies so large, especially with regard to flow nonuniformity? A possible explanation is that when the genetic algorithm searches for minimum flow resistance and minimum channel volume at the same time, it leads to configurations that look more and more like a single channel that runs from the upper-left corner to the lower-right corner (e.g., Fig. 5, network 23). All the channel volume is invested into this single channel, which has one diameter (i.e. no constrictions). If the genetic algorithm would be allowed to run *ad infinitum*, then it would generate a single zig-zag channel that descends along the diagonal–one channel and nothing else (see Fig. 8). This limiting design would have $\dot{m}_{min} = 0$ which means $\mu = \infty$ Furthermore, in the limit $\mathrm{Re} \to 0$ all the junction losses can be neglected, and the flow resistance of the zig-zag channel is equal to that of the L-shaped channel shown in Fig. 8. This limiting flow performance is easy to calculate:

$$\psi = 0.49, \quad \psi_{2D} = 0.032, \quad \mu = \infty \tag{8}$$

This result is shown to the right of Fig. 4. It serves as lower asymptote for the descending trend of ψ *versus* μ revealed by the data of Table 1 (see the dashed domain in Fig. 4).

The upper end of the dashed domain can also be explained. Consider the performance of the square grid shown in Fig. 9. Such a grid approximates the configurations that were used at the start of genetic modifications of the designs of Fig. 5, e.g., network 0. The square grid has channels with a single size, $D_1 = D_2$. The $\psi - \mu$ performance of this design can be evaluated with the same method as in Sections 2–4, and the results are

$$\psi = 8.1, \quad \mu = 7.3 \tag{9}$$

This point is marked with an asterisk in Fig. 4, and it is close to the upper end of the dashed domain. In fact, it is very close to the point of network 0, which also has a single channel size. If the porosity is defined according to Eq. (6), then the square-grid design has $\psi_{2D} = 43.1$ (and $\mu = 7.3$), as shown by the asterisk in Fig. 7. The conclusions based on Fig. 7 are the same as those based on Fig. 4.

6. Conclusion

The design performance reported as two curves in Figs. 4 and 7 is attractive from the point of view of endowing the flow architecture with two qualities, small flow resistance and modest flow nonuniformity. These results show all the designs, the good and the poor. There are even more designs than the ones that we have shown, and their $\psi - \mu$ performance data would fall above and to the right of our two curves. We did not spend time searching

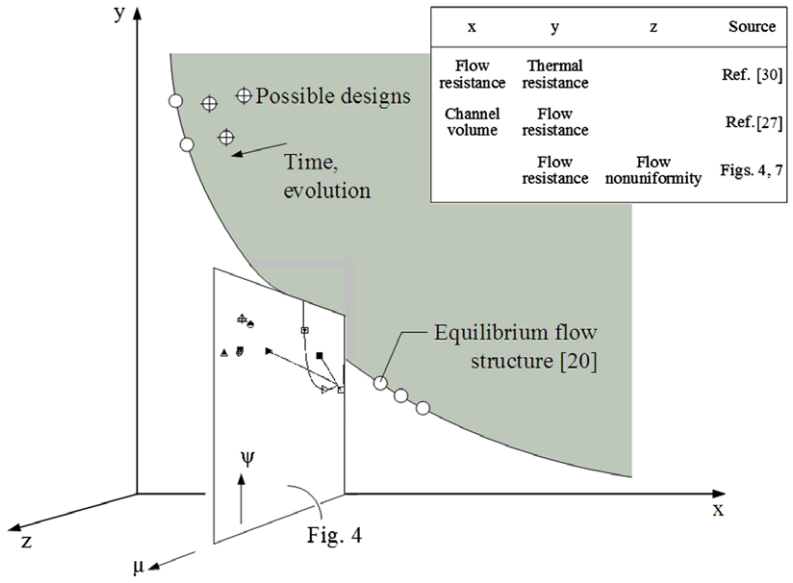

Fig. 6. The space for the design evolution of flow structures: from nonequilibrium structures to equilibrium structures.

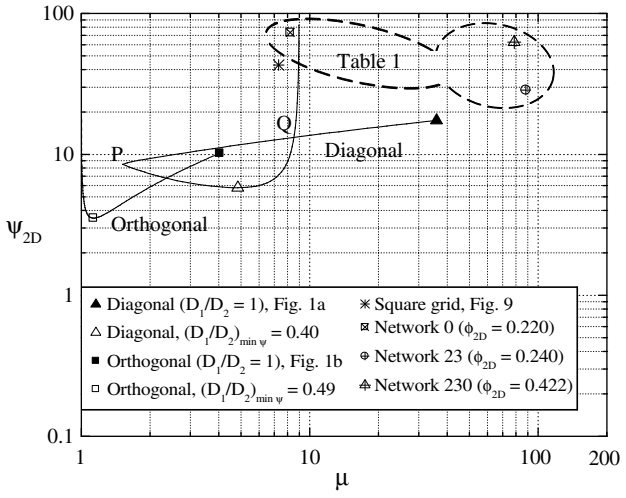

Fig. 7. The global flow resistance and nonuniformity of the designs of Fig. 1a and b, and Table 1, expressed in terms of the two-dimensional definitions (ϕ_{2D}, ψ_{2D}).

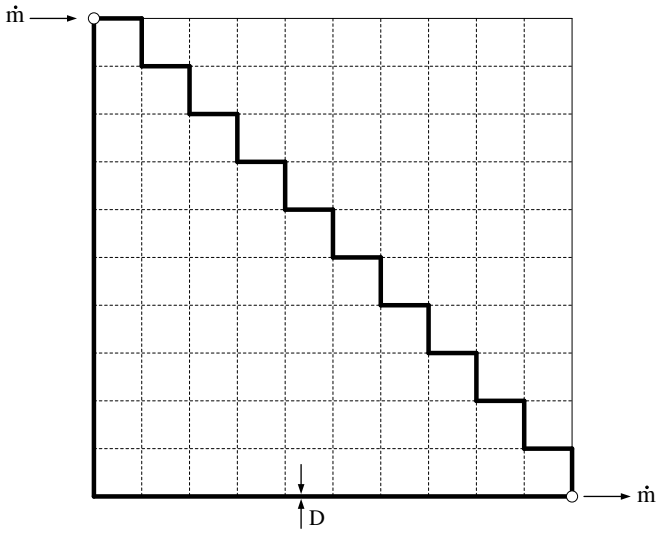

Fig. 8. The diagonal zig-zag and the equivalent *L*-shaped channel.

through this additional design domain because we knew from earlier constructal work [2,20] that certain configurations are effective for bathing an entire volume with one stream. Strategy is the design value of constructal theory.

Another conclusion is the effectiveness of the dimensionless group ψ (or ψ_{2D}) in describing the global flow resistance when the total void volume fraction is specified. Fig. 10 shows an additional example of the benefit of using this dimensionless group. The ordinate of the upper graph shows the group ψ_{2D}/ϕ_{2D}^4, which is proportional to the global flow resistance $\Delta P/\dot{m}$, as shown in Eq. (7). The four points (a)–(d) are from the search reported in Ref. [27], where two objectives were pursued: less $\Delta P/\dot{m}$ and less ϕ_{2D}. The design domain lies above the curve (a)–(d), in accordance with the *y*–*x* plane of Fig. 6.

The lower graph of Fig. 10 shows the same information by using ψ_{2D} on the ordinate. The results occupy a much narrower band: the vertical range spanned by the data is $\psi_{2D}(a)/\psi_{2D}(c) \cong 2.5$. On the upper graph, the corresponding ratio is $(\psi_{2D}/\phi_{2D}^4)(a)/(\psi_{2D}/\phi_{2D}^4)(b) \cong 15$. The lowest ψ_{2D} value of these data is 30, which is comparable with that of the grid design (Fig. 9) plotted in Fig. 7. The μ values of designs (a)–(d) of Ref. [27] are not available for a complete comparison on the field of Fig. 7. Furthermore, the points (a)–(d) will lie on a horizontal line if plotted on the plane $\psi - \phi$ [ϕ based on Eqs. (3) and (4)], instead of $\psi_{2D} - \phi_{2D}$.

The main conclusion of this work is that a complex flow architecture for volumetric functionality has more than one objective, and that the global performance is measured in several ways, each important. In Figs. 4 and 7 we used two measures at the same time (ψ, μ), and in Fig. 6 we sketched three. There are other flow qualities that a complex design has. One is resilience—what happens when one channel is blocked. To enhance this quality, recommended is the embedding of loops in the tree canopies of the design [25]. Another is the time and computational expense that the effort of design discovery requires [31]. All these qualities must be pursued simultaneously as the design evolution (i.e. our attention) is oriented toward multi-objective functionality distributed volumetrically through vascular smart materials.

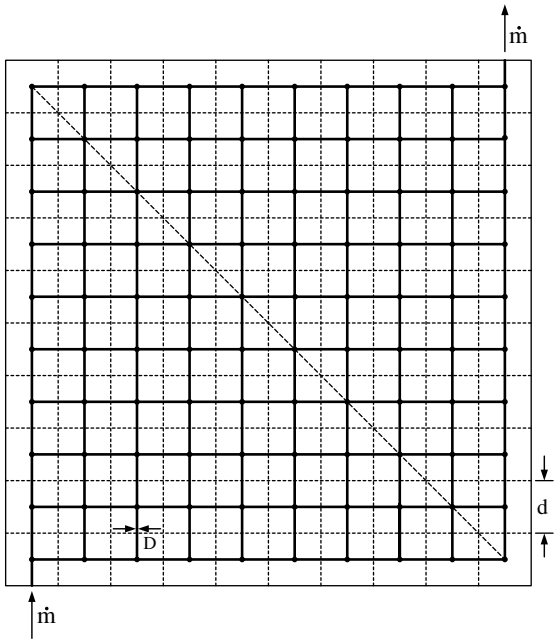

Fig. 9. Square grid with channels having a single diameter size.

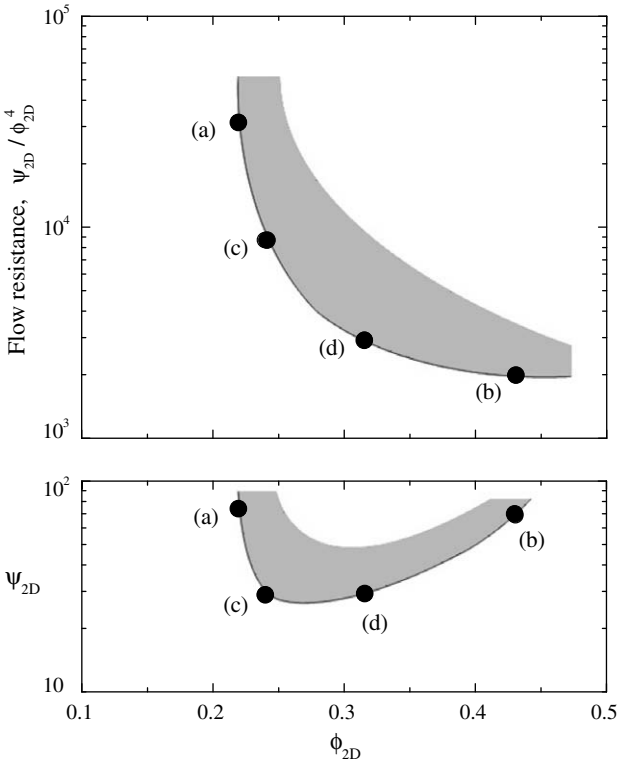

Fig. 10. The more compact presentation of flow performance data: flow resistance versus void fraction (upper graph), and the dimensionless group ψ_{2D} versus void fraction (lower graph).

The latest progress made with the constructal law in engineering design and design in nature is reviewed in a new book [32].

Acknowledgements

This research was supported by the Air Force Office of Scientific Research based on a MURI grant for the development of "Micro-Vascular Autonomic Composites" (University of Illinois at Urbana Champaign, Duke University, and University of California, Los Angeles). The authors thank Mr. A. Aragón and Prof. P. Geubelle for the advice on how to interpret the results reported in Ref. [27]. We thank Dr. David Moorhouse (Air Force Research Laboratory) for the advice and guidance that he gives us in this research direction. Jaedal Lee's work at Duke University was sponsored by the Korea Research Foundation Grant funded by the Korean Government (MOEHRD) (KRF-2006-612-D00011).

References

[1] T.L. Bergman, A. Faghri, R. Viskanta, Frontiers in transport phenomena research and education: energy systems, biological systems, security, information technology and nanotechnology, Int. J. Heat Mass Transfer 51 (2008) 4599–4613.
[2] A. Bejan, Shape and Structure, from Engineering to Nature, Cambridge University Press, Cambridge, UK, 2000.
[3] A. Bejan, M.R. Errera, Convective trees of fluid channels for volumetric cooling, Int. J. Heat Mass Transfer 43 (2000) 3105–3118.
[4] Y. Chen, P. Cheng, Heat transfer and pressure drop in fractal tree-like microchannel nets, Int. J. Heat Mass Transfer 45 (2002) 2643–2648.
[5] D.V. Pence, Reduced pumping power and wall temperature in microchannel heat sinks with fractal-like branching channel networks, Microscale Thermophys. Eng. 6 (2002) 319–330.
[6] G. Hernandez, J.K. Allen, F. Mistree, Platform design for customizable products as a problem of access in a geometric space, Eng. Optimiz. 35 (2003) 229–254.
[7] A.H. Reis, A.F. Miguel, M. Aydin, Constructal theory of flow architecture of the lungs, J. Med. Phys. 31 (2004) 1135–1140.
[8] K.E. Enfield, J.J. Siekas, D.V. Pence, Laminate mixing in microscale fractal-like merging channel networks, Microscale Thermophys. Eng. 8 (2004) 207–224.
[9] S.M. Senn, D. Poulikakos, Laminar mixing, heat transfer, and pressure drop in treelike microchannel nets and their application for thermal management in polymer electrolyte fuel cells, J. Power Sour. 130 (2004) 178–191.
[10] S.M. Senn, D. Poulikakos, Tree network channels as fluid distributors constructing double-staircase polymer electrolyte fuel cells, J. Appl. Phys. 96 (2004) 842–852.
[11] F. Lundell, B. Thonon, J.A. Gruss, Constructal Networks for Efficient Cooling/Heating, Second Conference on Microchannels and Minichannels, Rochester, NY, 2004.
[12] V.A.P. Raja, T. Basak, S.K. Das, Thermal performance of a multi-block heat exchanger designed on the basis of Bejan's constructal theory, Int. J. Heat Mass Transfer 51 (2008) 3582–3594.
[13] M. Lallemand, F. Ayela, M. Favre-Marinet, A. Gruss, D. Maillet, P. Marty, H. Peerhossaini, L. Tadrist, Thermal transfer in microchannels: applications to micro-exchangers, in: French Congress on Thermics, SFT 2005, Reims, 30 May–2 June 2005.
[14] N. Kockmann, T. Kiefer, M. Engler, P. Woias, Channel networks for optimal heat transfer and high throughput mixers, in: ECI International Conference on Heat Transfer and Fluid Flow in Microscale, Castelvecchio Pascoli, Italy, September 2005.
[15] Y.S. Muzychka, Constructal design of forced convection cooled microchannel heat sinks and heat exchangers, Int. J. Heat Mass Transfer 48 (2005) 3119–3127.
[16] X.-Q. Wang, A.S. Mujumdar, C. Yap, Numerical analysis of blockage and optimization of heat transfer performance of fractal-like microchannel nets, J. Electron. Packaging 128 (2006) 38–45.
[17] Y.S. Muzychka, Constructal multi-scale design of compact micro-tube heat sinks and heat exchangers, Int. J. Therm. Sci. 46 (2007) 245–252.
[18] A.H. Reis, Constructal theory: from engineering to physics, and how flow systems develop shape and structure, Appl. Mech. Rev. 59 (2006) 269–282.
[19] A. Bejan, S. Lorente, Constructal theory of generation of configuration in nature and engineering, J. Appl. Phys. 100 (2006) 041301.
[20] A. Bejan, S. Lorente, The constructal law and the thermodynamics of flow systems with configuration, Int. J. Heat Mass Transfer 47 (2004) 3203–3214.
[21] S.W. Kim, S. Lorente, A. Bejan, Vascularized materials: tree-shaped flow architectures matched canopy to canopy, J. Appl. Phys. 100 (2006) 063525.
[22] J. Lee, S. Kim, S. Lorente, A. Bejan, Vascularization with trees matched canopy to canopy: diagonal channels with multiple sizes, Int. J. Heat Mass Transfer 51 (2008) 2029–2040.
[23] E.R. Weibel, Symmorphosis: On Form and Function in Shaping Life, Harvard University Press, Harvard, MA, 2000. pp. 16–17.
[24] K. Schmidt-Nielsen, Scaling: Why is Animal Size So Important?, Cambridge University Press, Cambridge, 1984
[25] W. Wechsatol, S. Lorente, A. Bejan, Tree-shaped networks with loops, Int. J. Heat Mass Transfer 48 (2005) 573–583.
[26] A.K. da Silva, S. Lorente, A. Bejan, Constructal multi-scale tree-shaped heat exchangers, J. Appl. Phys. 96 (2004) 1709–1718.
[27] A.M. Aragón, C.J. Hansen, W. Wu, P.H. Geubelle, J. Lewis, S.R. White, Computational design and optimization of a biomimetic self-healing/cooling material, in: Proceedings of the Society of Photographic Instrumentation Engineers 6526, 652161G, 2007, pp. 1–10.
[28] S. Lorente, A. Bejan, Svelteness freedom to morph and constructal multi-scale flow structures, Int. J. Therm. Sci. 44 (2005) 1123–1130.

[29] D. Therriault, S.R. White, J.A. Lewis, Chaotic mixing in three-dimensional microvascular networks fabricated by direct-write assembly, Nat. Mater. 2 (2003) 265–271.
[30] W. Wechsatol, S. Lorente, A. Bejan, Dendritic convection on a disk, Int. J. Heat Mass Transfer 46 (2003) 4381–4391.
[31] W. Wechsatol, S. Lorente, A. Bejan, Tree-shaped flow architectures: strategies for increasing speed and accuracy, Numer. Heat Transfer Part A 48 (2005) 731–744.
[32] A. Bejan, S. Lorente, Design with Constructal Theory, Wiley, Hoboken, NJ, 2008.